Received: 22 February 2017 | Accepted: 4 May 2017

DOI: 10.1111/jace.14980

ORIGINAL ARTICLE

Journal of the American Ceramic Society

Processing YAG/α-Al_2O_3 composites via reactive sintering Y_2O_3/Al_2O_3 NP mixtures. A superior alternative to bottom up processing using atomically mixed $YAlO_x$ NPs

Richard M. Laine | **Nathan J. Taylor** | **Sandra Stangeland-Molo**

Department of Materials Science and Engineering, University of Michigan, Ann Arbor, Michigan

Correspondence
Richard M. Laine, Department of Materials Science and Engineering, University of Michigan, Ann Arbor, MI.
Email: talsdad@umich.edu

Funding information
Directorate for Engineering, Grant/Award Number: DMR Grant 1105361; NSF, Grant/Award Number: 1105361

Abstract

This effort contrasts "bottom-up" processing of YAG/α-Al_2O_3 composites where both elements (as 40-50 nm APSs nanopowders) are present at close to atomic mixing with reactive sintering where ball-milled mixtures of the individual nanopowders (40-50 nm APSs) give uniform elemental mixing at length scales closer to 100-800 nm with correspondingly much longer diffusion distances. In contrast to expectations, densification with control of final grain sizes is best effected using reactive sintering. Thus, reactive sintering to densities ≥95% occurs at only 1500°C with final grain sizes of ≈1000 nm for all samples. In contrast "bottom up" processing to ≥95% densities is only achieved at 1600°C, and with final grain sizes of 1700 nm. The reason for this unexpected behavior is that YAG phase forms early in the bottom up approach greatly inhibiting diffusion promoted densification. In contrast, in reactive sintering, YAG is prevented from forming because of the longer diffusion distances such that densification occurs prior to full conversion of the Y_2O_3 component to YAG. The found hardness values are statistically superior to literature values for composites near the known eutectic composition. In an accompanying paper, the addition of a third component reverses this behavior.

KEYWORDS

combustion synthesis, nanoparticles, processing, reaction sintering, yttrium aluminum garnet

1 | INTRODUCTION

Traditional methods of processing composite ceramic materials can follow multiple pathways. The simplest being co-milling of desired components with proven dispersants and binders and thereafter casting and sintering monoliths targeting final densities >95% to ensure superior mechanical properties. While this approach often succeeds, it also can generate final products with large average grain sizes (AGSs >5-10 μm) coincident with large critical flaws because of the high temperatures and/or long processing times required to achieve high final densities. This is especially true for efforts that explore the use of pressureless sintering.

Efforts to escape this demanding approach gave rise to chemical (sol-gel and polymer precursor) processing routes wherein atomic or near-atomic mixing of the target components was optimal.[1,2] The incentive was to minimize diffusion distances thereby minimizing processing times and/or temperatures, providing superior control of final densities, AGSs and therefore properties. Although this "bottom up" approach to processing works for multiple ceramic systems, it does not always work as we recently demonstrated.[3,4]

One clear impediment to its success arises when atomic mixing leads to very stable intermediate phases that resist further densification because of very low self-diffusion rates. Low diffusion rates thereby mandate higher sintering

temperatures or longer times arriving at the same final AGSs and flaw size distributions as a traditional approach.

For example, the bottom up approach using single phase nanopowders (NPs) fails for atomically mixed $Y_3Al_5O_{12}$ based ceramics because YAG exhibits very low diffusion rates. Such rates greatly inhibit further densification (Figure 1A) unless one resorts to much higher processing temperatures. Higher temperatures lead to excessive grain growth belying the utility of using bottom up NP processing.[3] In contrast, reactive sintering (Figure 1B) limits the rate of formation of YAG to later stages in the sintering process allowing full densification under much less demanding conditions giving finer control of final AGSs, flaw sizes and therefore properties.

A second example explored phase segregation coincident with densification in spinel NPs of composition $(NiO)_{0.25}(Al_2O_3)_{0.75}$ targeting formation of $(NiAl_2O_4)_{0.25}(Al_2O_3)_{0.50}$ composites. In this system, a comparison of the densification and final AGSs obtained at ≈95% density were identical to those obtained using mixtures of nano-$NiAl_2O_4$ spinel and nano-δ-Al_2O_3.[4] In this instance, the final target density mandated sintering conditions sufficient to drive extensive grain growth in the atomically mixed materials.

Thus, it is of considerable importance to delineate the basic processes involved in phase separation and densification on sintering these NP systems. We present here the first of several papers targeting the elucidation of such processes with initial studies targeting fine-grained YAG/α-Al_2O_3 composites. This work serves as a prelude to developing thin films of the same or similar materials for structural applications but also for processing porous membranes for catalyst applications as suggested by Figures 2 and 3. These studies are enabled using liquid feed-flame spray pyrolysis (LF-FSP) to produce a wide variety of single and mixed-metal oxide NPs in sufficient quantities (>30 g/h) to allow extensive processing studies.

In the LF-FSP process metalloorganic precursors are dissolved in alcohols in the desired composition at 1-10 wt % ceramic loading and aerosolized with O_2.[3-6] Typical precursors include metal alkoxides, carboxylates, or β-diketonates. The aerosol is ignited using methane/O_2 pilot torches generating flames at temperatures of 900°C-1500°C. The resultant gas phase species are rapidly (<100 milliseconds) quenched forming NPs with compositions essentially identical to the precursor feed which are collected downstream in electrostatic precipitators.[3-6]

Rapid quenching generates atomically mixed NPs that are typically agglomerated but minimally aggregated with specific surface areas (SSAs) of 30-120 m^2/g and average particle sizes (APSs) of 20-100 nm. In contrast to LF-FSP, other oxide NP synthesis methods such as coprecipitation and sol-gel processing often have lower degrees of mixing due to inhomogeneous rates of precipitation or hydrolysis, respectively.[7] LF-FSP is scalable and is well-studied.[3-6,8,9]

The YAG/α-Al_2O_3 composite system, especially the eutectic, shows promise as a high-temperature structural material in oxidizing environments.[10-13] A number of processing approaches to Al_2O_3-YAG (AY) composites have been used. Schehl et al. describe the utility of using yttrium alkoxide doping to pin exaggerated grain growth in α-Al_2O_3 through YAG phase formation along grain boundaries.[14] The resultant micro/nano composites had well dispersed 200 nm YAG particles at α-Al_2O_3 grain boundaries. Sommer et al. produced 5, 10, and 15 vol% AY composites from both alkoxide coated Al_2O_3 powders and mixtures of YAG and Al_2O_3 NPs.[15] In their work, composites sintered at 1500°C for 3 hours had theoretical densities that dropped from 98% to 94% TD as YAG content increased from 5 to 20 vol%. Both approaches produced composites with grains in the 3-5 μm size range.

Waku et al. synthesized eutectic composition, 45 vol% (80 mol%) AY composites from submicron Y_2O_3 and α-Al_2O_3 powders.[16] These composites exhibited a sharp

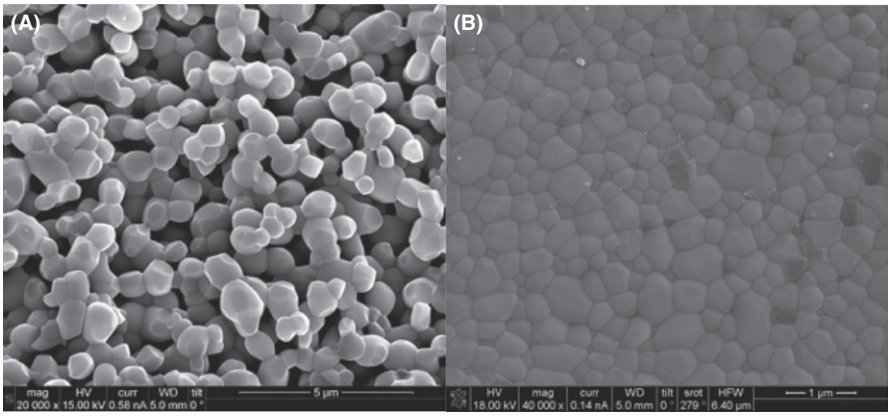

FIGURE 1 SEM of fracture surface of (A) $Y_3Al_5O_{12}$ nanocomposite composition (70% dense); (B) ball milled nano Y_2O_3–Al_2O_3 of same composition (>96% dense): 2-step heated to 1500°C/1300°C[3]

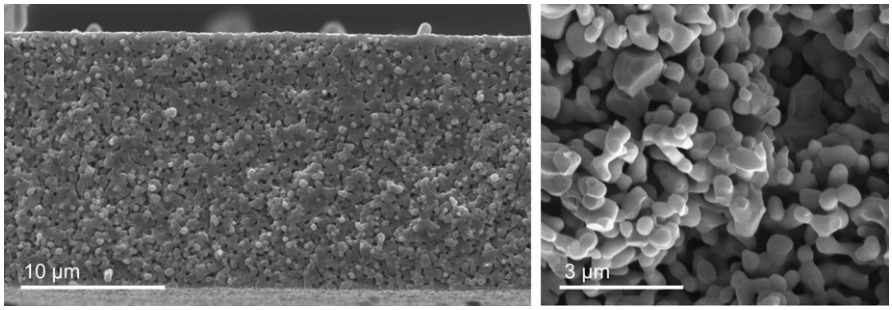

FIGURE 2 Sintering a $NiAl_2O_4$–Y_2O_3 film at 1400°C/1 hours/20% H_2–N_2. (Ni T_m=1450°C) producing a porous YAG/Ni metal composite (E. Yi and R. M. Laine, unpublished work)

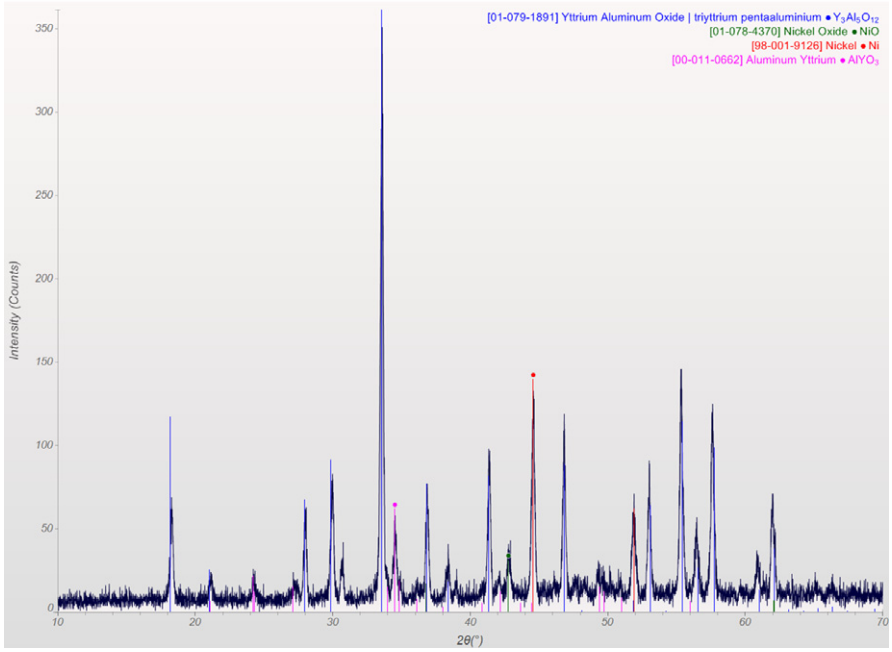

FIGURE 3 XRD of Figure 2 film. Ni metal and YAG are main crystalline phases, suggesting Al_2O_3 from spinel reacts with Y_2O_3. Small amount of $YAlO_3$ observed due to off stoichiometry or incomplete reaction (E. Yi and R. M. Laine, unpublished work) [Color figure can be viewed at wileyonlinelibrary.com]

reduction in flexural strength above 1000°C, likely due to amorphous material at grain boundaries. Palmero et al. produced 50 vol% AY composites from NPs produced by the reverse-strike-precipitation method.[17] Mechanical activation of the reverse-strike powders by planetary milling gave powders that sintered to 98% theoretical density (TD) after 2 hours at 1420°C with AGSs <200 nm. No mechanical properties were reported.

2 | EXPERIMENTAL PROCEDURE

2.1 | Materials

Yttrium propionate was prepared by the dissolution of $Y_2(CO_3)_3$ or Y_2O_3 (PIDC, Ann Arbor, MI) in propionic acid (Acros Organics, Geel, Belgium). Approximately 200 g (0.885 mol Y_2O_3) of starting material and 1 L (13.3 mol) of propionic acid was placed into a 3 L round bottom flask with magnetic stirring under dry N_2. The reaction was heated to 120°C for 10 hours, distilling off water. Full dissolution of the starting material into the propionic acid produces a yellow liquid, the reaction was then heated to 145°C to distill off excess acid. Care must be taken to ensure that some liquid remains at the end of the distillation or the product will decompose. The reaction was cooled, and yttrium propionate precipitated from the supersaturated solution. Typical ceramic yields determined by TGA for yttrium propionate used in the course of these studies were 34%-37%, consistent with the 36.6% theoretical ceramic yield for $Y(O_2CCH_2CH_3)_3$.

Alumatrane was used as the precursor to all Al_2O_3 powders produced in the course of this study. Aluminum tri-*sec*-butoxide (870 g, 3.53 mol) was added to a 5 L mechanically stirred reactor under dry N_2 flow. Triethanolamine (631 g, 4.23 mol) was slowly added with an addition funnel. The reaction is exothermic, so triethanolamine was slowly added to maintain a temperature less than 80°C. The byproduct butanol was distilled off and the resulting viscous alumatrane was dissolved in excess ethanol and the ceramic yield of the resulting solution was determined by TGA as described previously.[6]

2.2 | NP synthesis

Precursors were dissolved in anhydrous ethanol (Decon Labs, King of Prussia, PA) and diluted to 1-5 wt% ceramic

yield as measured by TGA The precursor solutions are fed at 50-100 mL/min into an atomizing nozzle using O_2 at 80 psi and a flow rate of 3.5 mol/min. The atomized droplets are ignited by ceramic methane/O_2 torches 40 mm from the nozzle face. Four separate nozzles feed shield gas, which envelops the flame, providing mixing to the turbulent flame and ensuring complete combustion.[3-6,9]

NPs are drawn downstream of the combustion chamber by an exhaust system, providing 5-8 m^3/min of exhaust. NPs entrained in the exhaust travel through two separate 120 cm aluminum tubes, which serve as electrostatic precipitators. Voltage is generated by a 10 kV AC oil burning furnace spark transformer. The output voltage is converted to DC with a custom bridge rectifier. Voltage is adjusted to provide maximum potential without arcing. Figure 4 provides a schematic of the flame spray pyrolysis apparatus.

NPs processed for compaction into ceramic bodies typically follow the following procedure. Approximately 10 g of as-produced NPs are ball milled with 2 wt% bicine in 300 mL of anhydrous ethanol with 0.5 mm yttrium stabilized ZrO_2, 3 mm yttrium stabilized ZrO_2, or 3 mm 99% Al_2O_3 media for 24 hours. After 24 hours of milling, the suspension is ultrasonicated for 20 minutes at 100 W using a Vibracell VC-505 ultrasonic horn (Sonics & Materials, Newtown, CT). The suspension is then allowed to settle for 24 hours and decanted to remove large settled particles. The suspension is dried, ground, and sieved though 75 μm polypropylene mesh. The powder is redispersed in anhydrous ethanol with 4 wt% binder, typically polyethylene glycol (PEG) with a M_w=3400. The suspension is then ultrasonicated for 20 minutes at 100 W of power. The suspension is then dried, ground, and sieved through 20 μm polypropylene mesh.

2.3 | Pellet formation

Sieved powders are loaded into a 14.7 mm tungsten carbide die and pressed to 14 MPa to for 3 minutes to produce 700-1000 mg cylindrical pellets. Stearic acid is used as a die lubricant. Pellets are then vacuum sealed into latex gloves and cold isostatic pressed to 200 MPa in an Autoclave Engineers CIP (Avure, Lewis Center, OH) to 200 MPa for 30 minutes. A typical pressure building and release rate is 10 MPa/min.

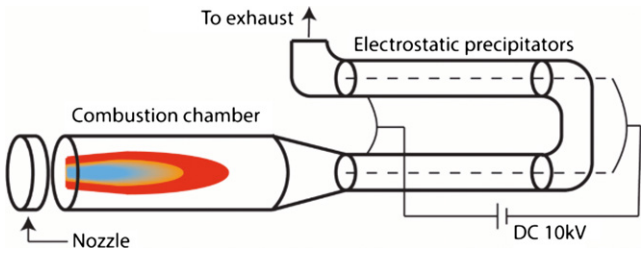

FIGURE 4 General schematic of the flame spray pyrolysis apparatus [Color figure can be viewed at wileyonlinelibrary.com]

2.4 | Thermal processing

Pellets are typically burned out 800°C for 4 hours in dry flowing air, with a ramp rate of 3°C/min. Burnout and sintering up to 1100°C is conducted in a BlueM (Thermo Fisher Scintific, Waltham, MA) tube furnace with a sealed quartz tube. Sintering from 1100°C to 1500°C is conducted in an MTI GSL-1600X (MTI Corporation, Richmond, CA) tube furnace. For sintering from 1500°C-1600°C, a BlueM muffle furnace is used.

2.4.1 | Pellet densities

Pellets were first boiled for 4 hours in deionized water, then were left for 24 hours in room temperature water. Measurements were performed using an Archimedes density kit for an Ohaus Voyager Pro balance, with a sensitivity of 0.1 mg.

2.5 | Grain size measurements

Dense ceramic samples were polished with standard ceramographic techniques. Polished samples were thermally etched at a temperature 50°C under the sintering temperature for 30 minutes. ImageJ (NIH, Bethesda, MD) was used for grain size measurements. Two different grain size measurement techniques were used. For nanocomposite materials or composites with relatively simple grain size distributions, the lineal intercept method was used across greater than 500 grain intercepts on at least five images. For composites with differing grain size distributions, at least 250 grains of each material were measured in ImageJ and adjusted by a proportionality factor of 1.56 for random slices through tetradecahedral grains.

2.6 | General characterization techniques

X-ray diffraction (XRD) was performed on a Rigaku rotating anode diffractometer (Rigaku USA, The Woodlands, TX) at 40 kV and 100 mA. Typical continuous scan ranges were from 10° to 70° 2θ at 2°/min with a 0.02° interval. XRD patterns were analyzed using JADE 2010. Rietveld refinements were conducted within JADE using the XX peak fitting model.

Scanning electron microscopy (SEM) was performed using a FEI Nova Nanolab dualbeam SEM/FIB or FEI Quanta 200 SEM/FIB (FEI Corporation, Hillsboro, OR). Typical accelerating voltages were 5-20 kV, depending on sample conditions. Powder samples (50 mg) were ultrasonicated in 20 mL

of ethanol and dropped onto SEM sample stubs. Pellets were mounted on sample stubs with copper tape.

Transmission electron microscopy (TEM) was performed using a JEOL 3011 HREM (JEOL Ltd., Tokyo, Japan) at 300 kV. Powder (10 mg) was dispersed in 20 mL ethanol and wicked through a 400 mesh carbon coated copper grid.

Thermogravimetric analysis/differential thermal analysis (TGA/DTA) was performed on a TA Instruments Q600 TGA/SDT (TA Instruments, New Castle, DE). Precursor ceramic yields were determined by experimental runs at 10°C/min to 1000°C. Thermal behavior of ceramic particles or pellets was characterized by sample runs at 10°C/min to 1400°C. All experiments were performed with dry air flowing at 60 mL/min.

Surface area analyses were run on a ASAP 2020 sorption analyzer (Micromeritics, Norcross, GA). Samples were degassed for 8 hours at 400°C under vacuum. An 11 point BET method analysis was conducted on 200 mg samples at relative pressures of 0.05-0.35. Nitrogen was used as the adsorbate gas and analysis was conducted in liquid nitrogen. Average particle sizes (APSs) were derived from BET SSAs per the following, where ρ is the particle density.

Formula for particle size for spherical particles from SSA.

$$d = \frac{6}{(\mathrm{SSA}) * \rho}$$

Dilatometry analyses were conducted using a Dilatronic II single pushrod dilatometer (Theta Industries, Port Washington, NY). Linear displacement was observed by a linear variable differential transformer (LVDT) and recorded by a custom LabView program. Constant heating rate experiments were conducted from room temperature to 1500°C with a 10°C/min ramp rate in static air.

Vickers microhardness measurements were made using a Clark CM-400AT equipped for Vickers hardness measurements. All measurements were taken at a load of 500 g. Values given are an average of at least ten separate indentation sites.

Diffuse reflectance infrared Fourier transform spectroscopy (DRIFTS) samples were prepared by grinding 5 mg of NP with 400 mg of spectroscopy grade KBr. Samples were analyzed on a ThermoScientific Nicolet 6700 FTIR spectrometer (Thermo Fisher Scientific, Waltham, MA) under dry flowing nitrogen. Recorded spectra were an average of 60 scans at 400-4000 cm^{-1} with a resolution of ± 4 cm^{-1}. A KBr blank was used as a reference sample.

3 | RESULTS AND DISCUSSION

An important aspect of working with NPs is the length scale of mixing. As-produced single-phase NPs will have atomic mixing and thus minimum diffusion lengths. Balling milling NPs does not provide sufficient energy to create new surfaces, thus primary particles sizes are not reduced. Ball milling does break up agglomerates, and in this case, only mixes the powders. If perfectly mixed, the length scale of mixing would be the distance between two adjacent nanoparticles of Y_2O_3 and Al_2O_3. In practice, the length scale of homogeneous mixing provided by ball milling is *at least* the size of agglomerates that could be 100-800 nm in size. This is *at least two orders* of magnitude greater than atomically mixed NPs.

The major objective of the work reported here is to explore the utility of reactive sintering of mixtures of single oxide Y_2O_3 and Al_2O_3 NPs as a route to very fine-grained AY oxide composites and to compare this with a "bottom up" approach using nanocomposite, essentially atomically mixed $YAlO_x$ NPs of the same composition and APS. The secondary objective is to determine the effect the length scale of mixing in the original NP compact has on the final composite microstructure and mechanical properties. Two-phase materials were produced from both LF-FSP NPs synthesized at the desired compositions and LF-FSP NPs of the constituent oxides mixed by ball milling to study the effects of phase development and sintering on the final microstructure. As seen in Figure 1, we find drastically different sintering behavior and final grain sizes in YAG tubes produced with these two processing techniques, which we mainly attribute to the differences in phase development due to the initial length scale of mixing.

3.1 | Powder characterization

Three atomically mixed compositions were synthesized resulting in powders with the BET SSAs and calculated

TABLE 1 Composition and BET SSAs for YAG–Al_2O_3 starting materials and composites

mol% Y_2O_3	mol% Al_2O_3	mol% Al_2O_3	mol% YAG	wt% Al_2O_3	wt% YAG	vol% Al_2O_3	vol% YAG	BET m^2/g	APSs nm
11.5	88.5	90.0	10.0	60.8	39.2	63.9	36.1	41	41
18.5	81.5	80.4	19.6	41.4	58.6	44.6	55.4	38	44
25.3	74.7	65.8	34.2	24.9	75.1	27.4	72.6	53	23
0	100							65	26
100	0							53	23

APSs as well as those of the pure powders detailed in Table 1. The phase diagram Figure S1 indicates that 88.5 mol% Al_2O_3–Y_2O_3 corresponds to the YAG/α-Al_2O_3 eutectic at 45 vol% Al_2O_3, making it a popular composition in the literature for YAG/α-Al_2O_3 composites. Although our processing conditions do not access the eutectic T_m, we processed several powder composites at this composition. The other two compositions synthesized here are ca. ±7 mol% from this composition, and all three compositions are within the YAG/α-Al_2O_3 two phase region.

Reactive sintering of Y_2O_3 and Al_2O_3 NPs will be referred to as the mixed nanoparticle approach. Sintering of LF-FSP nanoparticles produced at the exact composition will be referred to as the nanocomposite approach. To avoid confusion, we will refer to the samples by their composition in vol% and mol% Al_2O_3 of the final composition. Both synthesis processes start from metastable states, so the final composition is used as the sample nomenclature to avoid confusion. As previously, we targeted densities 95% theoretical density (TD) as a starting point for hot isostatic pressing (HIPing) for final densification with limited grain growth, if needed.

NPs were synthesized under standard LF-FSP conditions. Figure 5 provides a SEM of 45 vol% (80 mol%) Al_2O_3 as-produced nanocomposite NP, and is typical of all powders produced in this study. Particles are all generally <100 nm, with no fraction of large particles present. Table 2 gives BET SSAs for powders produced in this study. APSs were calculated using ρ=3.58 g/cm^3, representative of a low-density Al_2O_3–Y_2O_3 amorphous material since the true density of the powder is unknown, likely giving APSs slightly larger than their true values, as a low density would reflect a higher surface area for an equivalent mass.[18] BET derived APSs are within 20-50 nm, so the differences in particle size between nanocomposite nanoparticle and mixed nanoparticles are likely negligible.

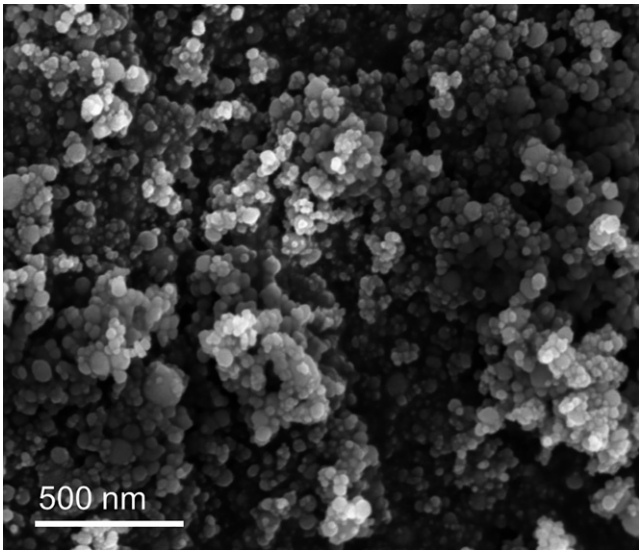

FIGURE 5 SEM of as-produced 45 vol% (80 mol%) Al_2O_3 nanocomposite nanoparticles

Figure 6 provides XRDs of as-produced nanocomposite powders. At 27 vol% Al_2O_3, δ-Al_2O_3, δ*-Al_2O_3, and hexagonal $YAlO_3$ are present, along with an amorphous hump centered at 33° 2θ. Hexagonal $YAlO_3$ is an intermediate phase, seen in almost all nano-YAG syntheses.[19,20] δ-Al_2O_3 and δ*-Al_2O_3 are transition-Al_2O_3 phases, typical of nano-Al_2O_3, and the two most common phases in LF-FSP Al_2O_3.[6] At 27 and 45 vol% (80 and 90 mol%) Al_2O_3, δ-Al_2O_3 is not seen, with only δ*-Al_2O_3 and hexagonal $YAlO_3$ observed. Both retain a significant amorphous fraction, indicated by an amorphous hump centered at 33° 2θ. Rietveld refinement of the XRD pattern for pure LF-FSP Y_2O_3 powders used in this study gives 77% cubic and 23% monoclinic. XRD shows LF-FSP Al_2O_3 to be a mixture of transition Al_2O_3 phases, mostly δ and δ*.

3.2 | Thermal analysis

Figure 7 shows DTA traces from TGA/DTA analyses of pellets after binder burnout. Dotted traces correspond to the mixed NP approach, and solid lines to nanocomposite NPs. It is important to note that YAP or $YAlO_3$ perovskite, and YAM, monoclinic $Y_4Al_2O_9$, are often intermediate products in YAG synthesis. Microdiffraction of TGA samples was used to identify the phase transformations associated with the exotherms. The increasing background for both 45 vol% (80 mol%) Al_2O_3 samples are a function of DTA baseline calibration and do not indicate any real thermal affect.

Note that an additional slight exotherm appears in the 27 vol% DTA at 1240°C. At present we cannot suggest a crystallization event that might cause this unless it is crystallization of α-Al_2O_3 which is in the region where such a crystallization might occur.[4]

All three nanocomposite NP samples show an exotherm at ≈935°C, corresponding to the transformation from hexagonal $YAlO_3$, δ-Al_2O_3, δ*-Al_2O_3 to YAP and/or YAM as indicated by XRD. In the 27 vol% (66 mol%) Al_2O_3 nanocomposite NP sample, an exotherm centered at 1070°C corresponds to the transformation to YAG. In the 45 vol% (80 mol%) Al_2O_3 nanocomposite NP sample, an exotherm around 1130°C corresponds to either the YAG and/or α-Al_2O_3 transformation, as both phases are present by XRD after the exotherm. In the 64 vol% (90 mol%) Al_2O_3 nanocomposite NP sample, an exotherm at 1140°C is typical of the transformation to α-Al_2O_3, and the exotherm around 1250°C corresponds to the transformation to YAG from YAP/YAP and Al_2O_3. All three compositions show similar YAP/YAM transformation temperatures, but note that the YAG transformation is suppressed as Al_2O_3 content

TABLE 2 AGSs and hardnesses for three compositions (NN=nanocomposite, Mix=mixed NPs)

	YAG [nm]	Al_2O_3 [nm]	%TD	Schedule	Hardness [GPA]
64 vol% Al_2O_3 NN	1800±310	1600±400	95	1500°C 8 h	18.6±1.7
64 vol% Al_2O_3 Mix	730±270	1100±460	95	1500°C 8 h	17.8±1.5
45 vol% Al_2O_3 NN	1800±370	1700±300	94	1600°C 4 h	16.5±1.7
45 vol% Al_2O_3 Mix	980±250	1000±280	95	1600°C 4 h	16.5±1.4
27 vol% Al_2O_3 NN	1700±420	1700±380	95	1600°C 4 h	15.1±1.3
27 vol% Al_2O_3 Mix	910±380	1000±320	95	1500°C 8 h	14.7±0.8

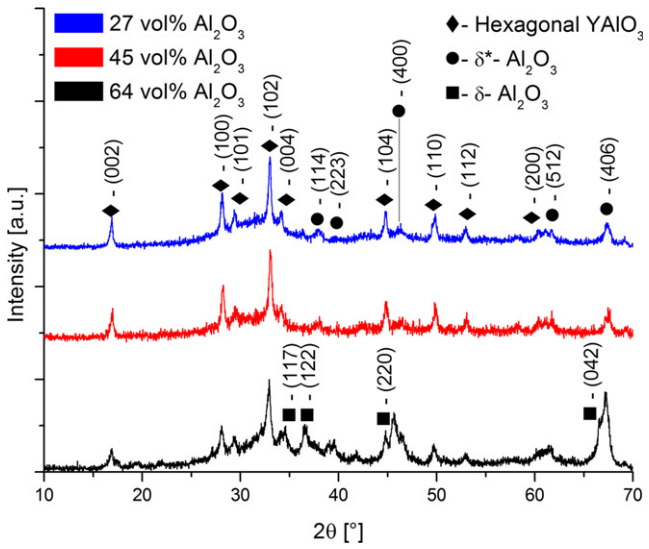

FIGURE 6 XRDs for 27, 45, and 64 vol% (66, 80, and 90 mol %) Al_2O_3 nanocomposite NPs [Color figure can be viewed at wileyonlinelibrary.com]

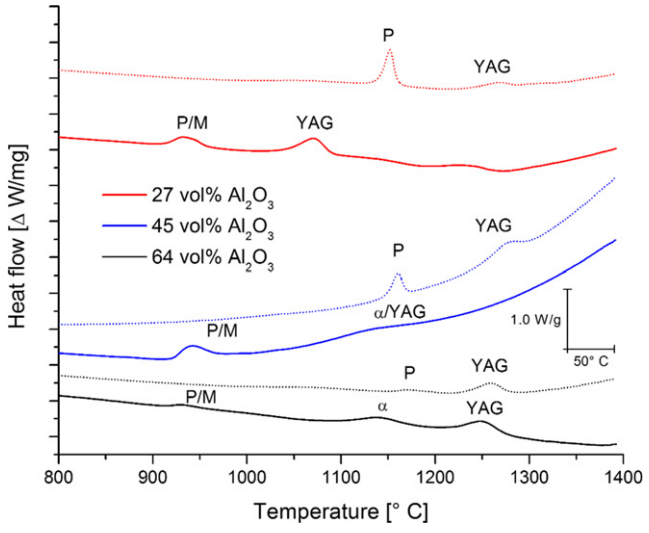

FIGURE 7 DTA traces of both mixed nanoparticle (dotted lines) and nanocomposite nanoparticle pellets (solid lines). (P=$YAlO_3$ perovskite, M=$Y_4Al_2O_9$ monoclinic, YAG=$Y_3Al_5O_{12}$, α=α-Al_2O_3) [Color figure can be viewed at wileyonlinelibrary.com]

increases. Per the phase diagram in Figure S1 both YAP and YAM are Y_2O_3-rich in comparison to YAG, so the transformation is diffusional. As Al_2O_3 content increases, the local composition is more Al_2O_3-rich, and the reaction to form YAG is delayed up to 180°C due to the diffusion necessary for YAG transformation. Since YAG formation impedes further diffusion and densification, this late transformation benefits densification as seen in the dilatometry results.

There is no indication from the XRD data that YAM actually forms. However, it is possible that under the processing conditions some YAM forms during heating but it is likely transient unlike what we see in similar systems.[3] Thus, we cautiously imply in the above discussion that it may be present by writing YAP/YAM transition.

Alternately, the reduction in YAG transformation temperature as Al_2O_3 increases suggests large YAP/YAM concentrations within a particle react with small amounts of Al_2O_3 more quickly than small amounts of YAP/YAM react with large amounts of Al_2O_3 to form YAG. This suggests a shift in the morphology of the particles as the composition is changed. Diffusional couples of Y_2O_3 and Al_2O_3 show the dominant mass transport is Al_2O_3 diffusion into Y_2O_3, so small islands of Al_2O_3 adjacent to YAP/YAM within a single particle may react more quickly to form YAG.[20] Hay studied YAG formation from diphasic Y_2O_3–Al_2O_3 gels and found diffusion of Al_2O_3 is rate-controlling in YAG formation.[21] At high loadings of Al_2O_3, the Al_2O_3 diffusion rate may be less than the diffusion rate into YAP/YAM, leading to the delay in YAG transformation seen here. Hay also observed the presence of YAG at temperatures as low as 800°C, indicating our DTA transformation temperatures are typical for this system.

In the mixed nanoparticle materials, an exotherm around 1160°C corresponds to the transformation to YAP, and the 1250°C-1270°C exotherm corresponds to the transformation to YAG, as seen by XRD, Figure 8. No change in thermal behavior is seen with compositional changes for the mixed NP processing approach. For mixed NPs, the reaction occurs as a diffusion couple between adjacent Y_2O_3 and Al_2O_3 NPs. The local Y_2O_3–Al_2O_3 interface is unchanged regardless of the global composition, so little change is seen in the DTA

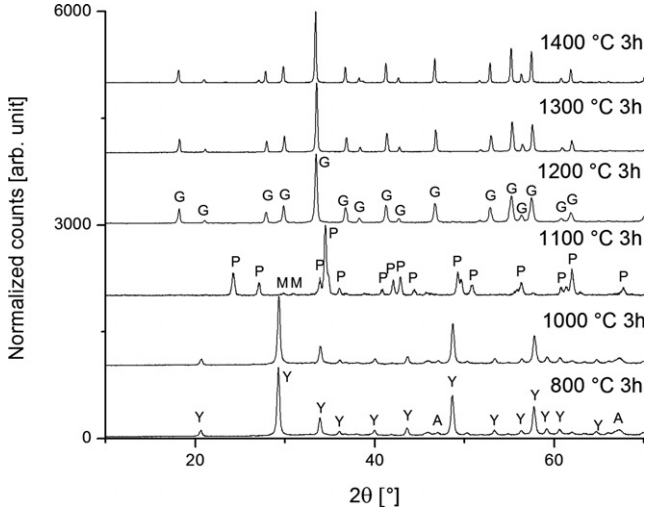

FIGURE 8 XRDs of 1:1 mixtures of Y_2O_3:Al_2O_3 nanopowder pellets on sintering for 3 h/air at 800°C-1400°C. Y=Y_2O_3, A=transition alumina, P=$YAlO_3$, M =$Y2Al_4O_9$, G=$Y_3Al_5O_{12}$ garnet

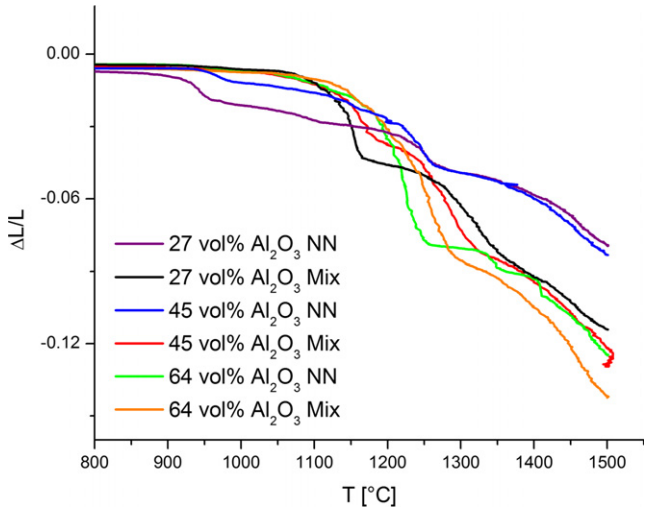

FIGURE 9 Dilatometry traces for all compositions studied [Color figure can be viewed at wileyonlinelibrary.com]

indicated phase transformations. In contrast, the local composition of the nanocomposite NPs closely matches the global composition. *This is an important observation because it indicates the length scale of mixing is approximately atomic vs the ball-milled NP samples*. As a result, the DTA indicates phase transformations are dependent on the global concentrations, basically indicating a "bulk property" effect.

3.3 | Dilatometry

Figure 9 provides dilatometric traces for all three compositions from both nanocomposite and mixed NP samples. All samples had green densities of 53%±2% TD. Both the mixed NP and nanocomposite 64 vol% (90 mol%) Al_2O_3 composites show the most densification up to 1500°C at 15% and 14% linear strain, respectively. Both the 45 and 27 vol% (80 and 66 mol%) Al_2O_3 mixed nanoparticle samples show similar densification levels of 12% and 13% linear strain. The nanocomposite 45 and 27 vol% Al_2O_3 samples show similar densification of ≈8% linear strain up to 1500°C, below that of the their respective mixed-NP counterparts. The nanocomposite sintering curves for 45 and 27 vol% (80 and 66 mol%) Al_2O_3 are similar to pure LF-FSP YAG NPs.[3]

This may indicate once YAG is the volume majority phase, the sintering of the continuous 3D connected YAG grains may be rate limiting for composite densification. The sintering of the Al_2O_3-YAG composites reflects the dilatometry curves.

3.4 | Final microstructure

Sintering efforts targeted densities of 95% TD reflecting a practical density with closed porosity for further processing by HIPing to still higher densities with minimal grain growth. Different sintering temperatures were used, but the data here are presented as an iso-density case. Figure 10 shows SEMs of polished and then thermally etched samples for all three compositions for both processing methods.

In a reflection of the higher densification at lower temperatures, the mixed nanoparticle composites sinter *to much finer grain sizes* than the nanocomposite nanoparticles at equivalent densities of 95%±1%TD. In general, the larger grain sizes observed for the nanocomposite NP case are likely a consequence of the higher sintering temperatures required. Table 2 gives the measured AGSs from the polished SEM micrographs. AGSs do not differ significantly with composition. All of the mixed nanoparticle composites have average grain sizes for both phases of ≈1000 nm. The nanocomposite nanoparticle samples have grain sizes for both phases of ≈1700 nm.

3.5 | Vickers microhardness

Microhardness data for each sample are also tabulated in Table 2. Larrea et al. suggest that the Al_2O_3 content dominates the hardness in YAG/α-Al_2O_3 eutectic composites. Our results fit well with this observation.[22] Higher hardness values are observed as Al_2O_3 volume fraction increases. No significant differences between the nanocomposite and mixed NP samples were observed. The hardness of bulk Al_2O_3 is commonly cited as 17.7 GPa, but values as high as 20 GPa have been obtained from NP processed Al_2O_3 with 1 μm AGS.[23] The observed values suggest that the critical flaw sizes in both types of materials are similar and *may be a consequence of sample polishing* (see work of Niihara et al.)[24] rather than offering a direct measure of the effects of AGSs. Future studies will address this issue.

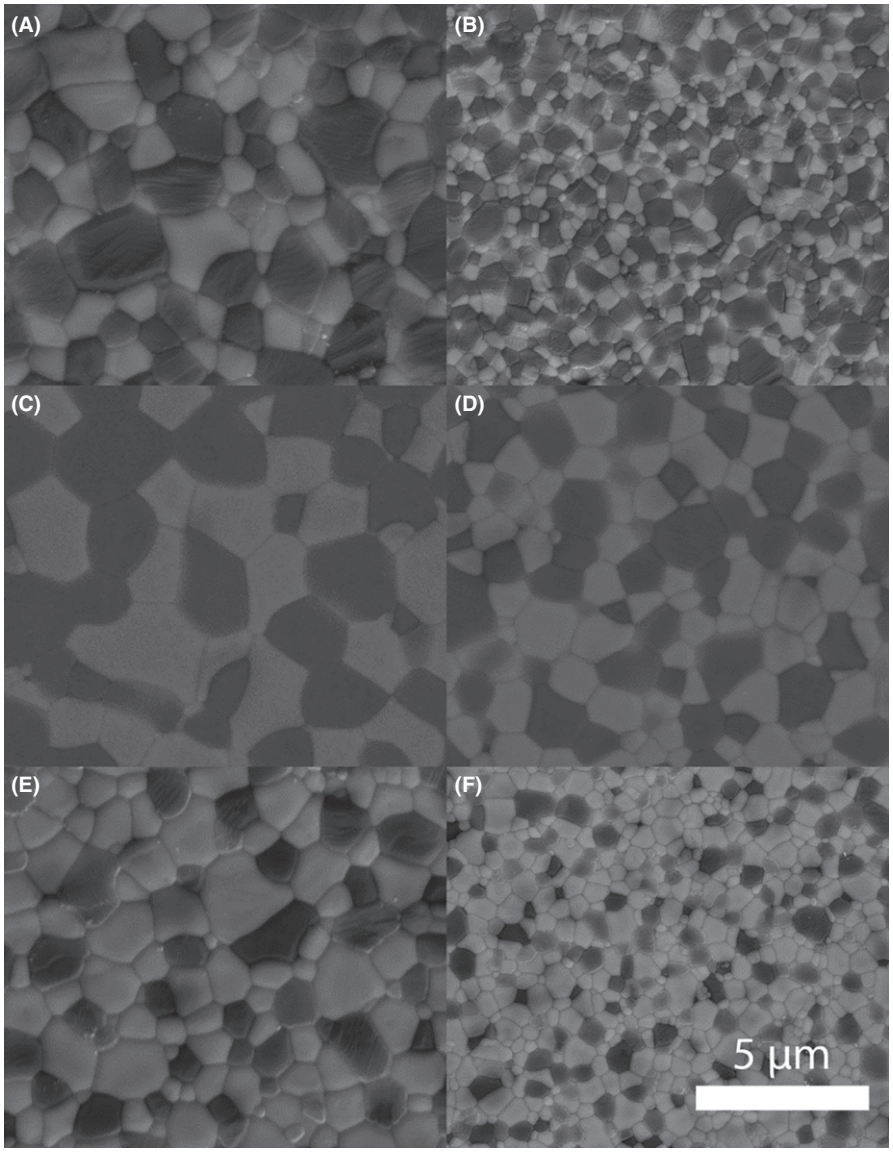

FIGURE 10 SEMs at 95%TD for (A) 64 vol% Al_2O_3 nanocomposite (B) 64 vol% Al_2O_3 mixed (C) 45 vol% Al_2O_3 nanocomposite (D) 45 vol% Al_2O_3 mixed (E) 27 vol% Al_2O_3 nanocomposite (F) 27 vol% Al_2O_3 mixed

The bulk Al_2O_3 hardness is equivalent to our 64 vol% (90 mol%) Al_2O_3 mixed NP sample, and below the nanocomposite NP sample of the same composition, but both are below the 20 GPa for NP derived Al_2O_3. For reference, Li and Gao obtained a hardness of 16.15 GPa for 75 vol% Al_2O_3-YAG composites.[25] Although these results suggest enhanced hardness due to a pseudo-Hall-Petch grain size effect, the high hardness values here may also be a consequence of the low loading used in microhardness testing.[26] Our microhardness testing used a load of 500 g, whereas it has been suggested that Vickers hardness tests for true hardness should be run using 5-10 kg loads. Comparative hardness studies with higher loads will be performed in the future to determine if a true grain size hardness effect is present. Again an alternative interpretation is that the fatal flaws in both materials are a consequence of surface finish from polishing of the test samples.[24] This also will be tested in future studies.

The nanocomposite NP processing scheme prevents densification, and as a result mixed nanoparticle reactive sintering provides finer grain sizes in 95% dense composites at all compositions tested. In the YAG/α-Al_2O_3 system, the mixed NP case provides finer microstructures, with no indication that particle mixing affected the final phase dispersion. The AGSs are consistent with literature, except for Palmero et al.[17] who found <200 nm AGSs from planetary milled powders. Although not well explored here, the finer grain sizes of the mixed NP samples may lead to superior mechanical properties both in bulk and in thin films, especially laminates.

4 | CONCLUSIONS

YAG/α-Al_2O_3 composites were prepared using two processing schemes, the mixing of the constituent oxide NPs, or mixed NPs, and single-phase NPs containing the overall

stoichiometry of the composite. In all cases, the mixed NP cases sinter to microstructures with *significantly* finer grain sizes than found with nanocomposite NPs at equivalent densities. As in our earlier work,[3,4] transformation to the YAG phase prevents low temperature densification in the single-phase nanoparticle materials supporting the idea that *the bottom up approach is not always the best approach* to processing selected composite materials not just single-phase materials.

In nanocomposite NPs, DTA indicates a significant reduction in the YAG nucleation temperature from 1250° to 1070°C as Y_2O_3 content increases. Since YAG forms by reaction of Al_2O_3 with YAP/YAM, this suggests the particle morphology offers smaller diffusion distances for rate-limiting Al_2O_3 species as Y_2O_3 content increases. In the mixed NP processing scheme, no change in the thermal behavior is seen with changing composition, consistent with a fixed reaction front between adjacent Al_2O_3 and Y_2O_3 nanoparticles.

Hardness testing showed no significant increase in the hardness between the nanocomposite and mixed NP processing schemes. Hardness did increase as the Al_2O_3 volume fraction increased, to a peak of 18.6±1.7 GPa for the 64 vol% Al_2O_3 nanocomposite NP sample. This value is above that of bulk Al_2O_3, but lower than that of some fine-grained Al_2O_3. Future testing with higher Vickers hardness loads should be performed to determine if we are seeing a true Hall-Petch type increase in hardness due to grain size.

These results are very important in processing fine-grained ceramic films given that finer grain sizes provide a more torturous path for crack propagation *if cracks propagate along grain boundaries.* An alternative explanation is that coincident with grain growth average flaw sizes also grow leading to poorer mechanical properties.

In terms of our long-term goals, finer grain sizes will also provide higher SSAs for porous membranes that can be used as catalyst support. In addition, finer grains in thin films provide flexibility suggesting superior mechanical properties as illustrated recently in our work on lithium ceramic electrolytes and nickel aluminate thin films (B. Liang, E. Yi and R. M. Laine, unpublished work; B. Liang, E. Yi, D. Jia, Y. Zhou, T. Sato, S. Noda and R. M. Laine, submitted).[5,27]

As we test the bottom-up approach to composite synthesis, we find mixed NP processing to be superior to the nanocomposite NP processing scheme. This runs contrary to the idea that controlling the composite composition at the finest possible length scale leads to the best composites. In addition, the results described here indicate powder processing is likely much more important than powder chemical homogeneity. Despite the advantage of the mixed nanoparticle approach, the AGSs are around 1 μm. To reduce the grain size into the nanometer range, we explored the addition of a third phase to both further pin grain boundary movement and provide lower temperature sintering. These studies are described elsewhere,[28] where we add a Y_2O_3 stabilized ZrO_2 phase to YAG/α-Al_2O_3 composites.

ACKNOWLEDGMENT

We are grateful for support of this work by NSF through DMR Grant 1105361.

REFERENCES

1. Brinker CJ, Scherer G. *Sol-Gel Science*. N.Y., N.Y.: Academic Press; 1991.
2. Laine RM, Sellinger A. Si-Containing Ceramic Precursors. In: Rappoport Z, Apeloig Y, eds. *The Chemistry of Organic Silicon Compounds*. Vol 2. London: J. Wiley & Sons Ltd.; 1998:2245-310.
3. Taylor NJ, Laine RM. Bottom up processing is not always optimal. YAG tubes. *Adv Func Mater*. 2014;24:1125-1132.
4. Taylor NJ, Pottebaum AJ, Uz V, Laine RM. The bottom up approach is not always the best processing method. Dense α-Al_2O_3/$NiAl_2O_4$ composites. *Adv Func Mater*. 2014;24:3392-3398.
5. Yi E, Wang W, Mohanty S, Kieffer J, Tamaki R, Laine RM. Materials that can replace liquid electrolytes in Li batteries: superionic conductivities in $Li_{1.7}Al_{0.3}Ti_{1.7}Si_{0.4}P_{2.6}O_{12}$. Processing combustion synthesized nanopowders to free standing thin films. *J Power Sources*. 2014;269:577-588.
6. Hinklin T, Toury B, Gervais C, et al. Liquid-feed flame spray pyrolysis of metalloorganic and inorganic alumina sources in the production of nanoalumina powders. *Chem Mater*. 2004;16:21-30.
7. Kakihana M. Invited review 'sol-gel' preparation of high temperature superconducting oxides. *J Sol-Gel Sci Technol*. 1996;6:7-55.
8. Pratsinis SE. Flame aerosol synthesis of ceramic powders. *Prog Energy Combust Sci*. 1998;24:197-219.
9. Sutorik AC, Laine RM, Marchal JC, Johns T, Hinklin T. Mixed-metal oxide particles by liquid feed-flame spray pyrolysis of oxide precursors in oxygenated solvents. US Patent 7220398 issued May 22, 2007.
10. Parthasarathy TA, Mah T-II, Matson LE. Processing, structure and properties of alumina-YAG eutectic composites. *J Ceram Proc Res*, 2004;5:80-390.
11. Hirano K. Application of eutectic composites to gas turbine system and fundamental fracture properties up to 1700. *J Eur Ceram Soc*. 2005;25:1191-1199.
12. Waku Y, Nakagawa N, Wakamoto T, Ohtsubo H, Shimizu K, Kohtoku Y. A ductile ceramic eutectic composite with high strength at 1873 K. *Nature*. 1997;389:49-52.
13. Llorca J, Orera VM. Directionally solidified eutectic ceramic oxides. *Prog Mater Sci*, 2006;51:711-809.
14. Schehl M, Díaz LA, Torrecillas R. Alumina nanocomposites from powder–alkoxide mixtures. *Acta Mater*. 2002;50:1125-1139.
15. Sommer F, Kern F, El-Maghraby HF, et al. Effect of preparation route on the properties of slip-casted Al_2O_3/YAG composites. *Ceram Int*. 2012;38:4819-4826.
16. Waku Y, Nakagawa N, Ohtsubo H, Mitani A, Shimizu K. Fracture and deformation behaviour of melt growth composites at very high temperatures. *J Mater Sci*. 2001;36:1585-1594.

17. Palmero P, Simone A, Esnouf C, Fantozzi G, Montanaro L. Comparison among different sintering routes for preparing alumina-YAG nanocomposites. *J Eur Ceram Soc*. 2006;26:941-947.
18. Wilding MC, Benmore CJ, McMillan PF. A neutron diffraction study of yttrium- and lanthanum-aluminate glasses. *J Non-Cryst Solids*. 2002;297:143-155.
19. Sim S-M, Keller KA, Mah T-I. Phase formation in yttrium aluminum garnet powders synthesized by chemical methods. *J Mater Sci*. 2000;35:713-717.
20. Glushkova VB, Krzhizhanovskaya VA, Egorova ON, Udalov YuP, Kachalova LP. Interaction of yttrium and aluminum-oxides. *Inorg Mater*. 1983;19:80-84.
21. Hay RS. Phase transformations and microstructure evolution in sol-gel derived yttrium-aluminum garnet films. *J Mater Res*. 1993;8:578-604.
22. Larrea A, Orera VM, Merino RI, Peña JI. Microstructure and mechanical properties of Al_2O_3–YSZ and Al_2O_3–YAG directionally solidified eutectic plates. *J Eur Ceram Soc*. 2005;25:1419-1429.
23. Teng X, Liu H, Huang C. Effect of Al_2O_3 particle size on the mechanical properties of alumina-based ceramics. *Mater Sci Eng: A*. 2007;452–453:545-551.
24. Ohji T, Jeong Y-K, Choa Y-H, Niihara K. Strengthening and toughening mechanisms of ceramic nanocomposites. *J Am Ceram Soc*. 1998;81:1453-60. and references therein.
25. Li WQ, Gao L. Processing, microstructure and mechanical properties of 25 vol% YAG–Al_2O_3 nanocomposites. *Nanostructured Mater*. 1999;11:1073-1080.
26. Krell A. Comment: the effect of grain size on the mechanical and optical properties of spark plasma sintering-processed magnesium aluminate spinel $MgAl_2O_4$ (Rothaman et al.). *Int J Appl Ceram Technol*. 2015;12:E174-E175.
27. Yi E, Wang W, Kieffer J, Laine RM. Key parameters governing the densification of cubic-$Li_7La_3Zr_2O_{12}$ Li^+ conductors. *J Power Sources*. 2017;352:156-164.
28. Taylor NJ, Stangeland-Molo S, Laine RM. Comparing bottom up processing with reactive sintering. Processing routes to dense Al_2O_3–YAG–YSZ composites from single and three-phase nanoparticles (NPs). Bottom up processing wins this time. *J Am Ceram Soc* 2017. https://doi.org/10.1111/jace.14761

SUPPORTING INFORMATION

Additional Supporting Information may be found online in the supporting information tab for this article.

How to cite this article: Laine RM, Taylor NJ, Stangeland-Molo S. Processing YAG/α-Al_2O_3 composites via reactive sintering Y_2O_3/Al_2O_3 NP mixtures. A superior alternative to bottom up processing using atomically mixed $YAlO_x$ NPs. *J Am Ceram Soc*. 2017;100:4500–4510. https://doi.org/10.1111/jace.14980